Electronic Supplementary Information

Controllable Preparation of Cation Vacancy-Modulated Oxygen Defects $Mn_{2-x}P_2O_{7-y}$ Anodes to Enhance the Lithium Storage Performance

Zhengen Sun,[a] Ning Zhang,[a] Yanjun Cai,[a] Qingrong Kong,[a] Xiang Yao,[a] Hualing Tian,[a] Ziyun Ma,[a] Yang Zhang *[a] and Zhi Su *[b]

([a] *College of Chemistry and Chemical Engineering, Xinjiang Key Laboratory of Energy Storage and Photoelectroctalytic Materials, Xinjiang Normal University, Urumqi, 830054, Xinjiang, China)*

([b] Xinjiang University, Urumqi 830017, Xinjiang, P.R. China)

**Corresponding author: Yanjun Cai, Zhi Su*

Tel: +86-991-4332683; zyangxy@163.com, suzhi@xju.edu.cn (Z. Su)

Experimental

Synthesis

A mixture of 0.2 mol of $(CH_3COO)_2Mn$ and $NH_4H_2PO_4$ was ground for 15 min and added to a reactor containing 60 mL of C_2H_5OH, then heated to 180 ℃ for 12, 18, 24, 30, and 36 h, respectively. After cooling down to room temperature, the samples were dried in an oven at 80 ℃ for 12 h. The precursors were subsequently calcined under an Ar atmosphere (500 ℃ for 6 h, with a heating rate of 5 ℃ min^{-1}) to produce $Mn_2P_2O_{7-y}$, labelled as MPO-OV-1 through MPO-OV-5.

$Mn_{2-x}P_2O_{7-y}$ was synthesized similarly, with variations in the amount of $(CH_3COO)_2Mn$ (x = 0.2, 0.199, 0.197, 0.195, 0.193 and 0.191 mol, respectively).

Material characterization

Phase compositions of $Mn_{2-x}P_2O_{7-y}$ were characterized by X-ray diffraction (XRD; Bruker D8/Cu Kα radiation). Morphology analysis was conducted by utilizing scanning electron microscopy (SEM, Thermo scientific Apreo 2C) and transmission electron microscopy (TEM, H-600, Hitachi, Japan). The presence of unpaired electrons, free radicals, valence changes of metal ions and lattice defects of the materials can be detected by an electron paramagnetic resonance spectrometer (EPR, Bruker/A300). The electronic states of $Mn_2P_2O_{7-y}$ and $Mn_{1.93}P_2O_{7-y}$ were detected by X-ray photoelectron spectroscopy (XPS, PHI 5000 Versa Probe).

Electrochemical characterization

The electrode materials were typically prepared according to the following procedure: the active materials, polyvinylidene fluoride (PVDF) and acetylene black were mixed at a mass ration of 8:1:1 and ground in an agate mortar for 10 min, and then a certain amount of N-methyl pyrrolidone (NMP) is added to obtain the slurry mixture. Thereafter, this slurry was uniformly coated applied to a copper foil of a certain thickness. Airing at room temperature and then transferred to an oven and vacuum dried at 110 °C for 12 h. The dried copper foil was cut into 12 mm diameter discs to be used as anode. Celgard 2400 was used as the diaphragm, the electrolyte

was 1 mol L^{-1} of $LiPF_6$ that consisted of EC, DMC and EMC (1:1:1; V/V/V), and lithium metal was utilized as the counter electrode. The coin cells (2032) were assembled in a glove box in an argon atmosphere with a water/oxygen concentration of <100 ppm. Cyclic voltammetry curves and electrochemical impedance spectra (EIS) were accounted on a CHI-660C workstation with a sweep rate of 0.1 mV s^{-1}. Galvanostatic charge and discharge (GCD) processes were conducted on a Land (CT2001A China) at 0.01-3.00 V (versus Li^+/Li). The specific capacities of the electrodes were calculated according to the total mass of the composites, whereas the typical loading of the active material was about 0.85 mg cm^{-2}. All electrochemical tests were conducted at room temperature.

Table S1 Lattice constants of $Mn_2P_2O_{7-y}$ synthesized at different hydrothermal time.

Lattice constant	MPO-OV-1	MPO-OV-2	MPO-OV-3	MPO-OV-4	MPO-OV-5
a	6.59341	6.60340	6.61010	6.61627	6.60567
b	8.53957	8.54386	8.55671	8.56533	8.49183
c	4.43291	4.43507	4.44663	4.49879	4.44625
Vol	247.06000	247.57000	248.74000	249.11000	248.71000

Table S2 Lattice parameters of $Mn_{2-x}P_2O_{7-y}$.

Lattice parameter	$Mn_2P_2O_{7-y}$	$Mn_{1.99}P_2O_{7-y}$	$Mn_{1.97}P_2O_{7-y}$	$Mn_{1.95}P_2O_{7-y}$	$Mn_{1.93}P_2O_{7-y}$	$Mn_{1.91}P_2O_{7-y}$
a	6.6163	6.6193	6.6217	6.6298	6.6386	6.6203
b	8.5653	8.5790	8.5854	8.5919	8.6181	8.5818
c	4.4988	4.5172	4.5262	4.5332	4.5410	4.5209
Vol	249.1100	249.8400	250.5500	250.7500	251.2600	249.9500

The lattice parameters of $Mn_{2-x}P_2O_{7-y}$ in **Table S2** show a trend of increasing and then decreasing, which indicates that manganese defects are present in the compounds, the occurrence of manganese defects can increase the interlayer spacing and accelerate the charge transfer process, thus facilitating the intercalation/deintercalation process and increasing the migration channels of ions [S1-S6]. Whereas the lattice parameter starts to decrease when Mn:P is 1.91:2, suggesting that excessive manganese defects will lead to a lattice distortion or collapse and reduce the ion embedding sites [S7, S8].

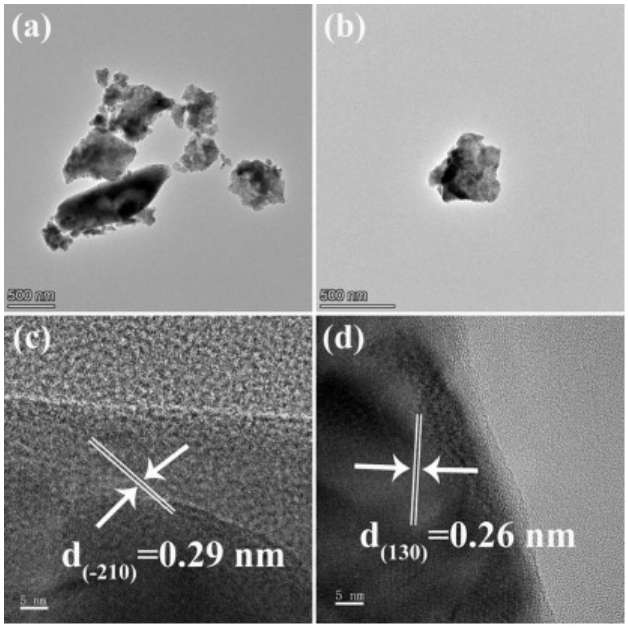

Fig. S1 TEM and HREM images of $Mn_2P_2O_{7-y}$ (a, c) and $Mn_{1.93}P_2O_{7-y}$ (b, d).

The morphological characteristics of $Mn_2P_2O_{7-y}$ and $Mn_{1.93}P_2O_{7-y}$ were presented in **Fig.S1**. After the high temperature calcination treatment, the samples take on the irregular lumps with a certain degree of agglomeration. Additionally, clear lattice stripes appeared in the HRTEM of $Mn_2P_2O_{7-y}$ (**Fig.S1c**) and $Mn_{1.93}P_2O_{7-y}$ (**Fig.S1d**), and the interplanar spacing of the two was calculated as 0.29 and 0.26 nm, corresponding to the (-210) and (130) crystal planes of $Mn_2P_2O_{7-y}$ (PDF#29-0891), respectively.

Table S3 Rate capabilities of $Mn_2P_2O_{7-y}$ synthesized under different solvothermal reaction time (mA h g^{-1}).

Samples	0.2	0.5	1	2	5	1	0.5	0.2	1 A g^{-1}
MPO-OV-1	610.5	372.0	310.5	208.7	22.2	263.0	261.5	282.7	230.6
MPO-OV-2	810.8	420.2	344.5	240.6	69.4	257.7	288.3	324.2	247.2
MPO-OV-3	890.5	422.4	328.8	217.2	56.9	271.5	295.5	324.2	277.0
MPO-OV-4	1224.0	466.4	367.1	271.7	100.0	231.2	295.1	374.5	323.2
MPO-OV-5	682.6	390.8	320.1	191.1	51.1	252.9	296.7	328.9	256.9

Table S4 Rate capabilities of $Mn_{2-x}P_2O_{7-y}$ (mA h g^{-1}).

Samples	0.2	0.5	1	2	5	1	0.5	0.2 A g^{-1}
$Mn_2P_2O_{7-y}$	1224.0	466.4	367.1	271.7	100.0	231.2	295.1	374.5
$Mn_{1.99}P_2O_{7-y}$	1137.1	479.9	377.6	281.7	123.6	251.4	303.4	397.9
$Mn_{1.97}P_2O_{7-y}$	1160.9	464.4	380.9	291.7	155.6	266.2	332.9	415.9
$Mn_{1.95}P_2O_{7-y}$	1080.6	470.5	387.5	293.8	157.2	282.2	341.9	420.4
$Mn_{1.93}P_2O_{7-y}$	1238.8	565.2	451.6	336.1	172.2	304.4	384.5	474.2
$Mn_{1.91}P_2O_{7-y}$	1036.3	477.3	385.9	292.8	150.0	264.8	328.9	406.8

Table S5 Cyclic performances of $Mn_2P_2O_{7-y}$ (0.2 A g^{-1}) synthesized under different solvothermal reaction time (mA h g^{-1}).

	MPO-OV-1	MPO-OV-2	MPO-OV-3	MPO-OV-4	MPO-OV-5
1st discharge specific capacity	588.4	702.1	816.5	973.0	757.6
1st charge specific capacity	224.2	293.2	396.0	412.1	370.7
80th discharge specific capacity	162.7	192.4	311.9	329.4	291.6
80th charge specific capacity	160.2	187.9	307.4	326.7	283.3
Discharge capacity retention rate	27.7%	27.4%	38.2%	33.9%	38.5%

Table S6 Comparison of electrochemical performances of pyrophosphate anodes in the open literatures.

Materials	Current density ($mA\ g^{-1}$)	Cycle numbers	Capacity ($mA\ h\ g^{-1}$)	Ref
SnP_2O_7	200	80	230	[S9]
$Mn_2P_2O_7$	1000	300	215.6	[S10]
$Cu_2(OH)PO_4$	500	—	340	[S11]
$Fe_{0.5}Ti_2(PO_4)_3$	50	25	350	[S12]
$LiVP_2O_7$/C	120	100	350	[S13]
$Mn_2P_2O_7$	50	35	160	[S14]
$CoNiP_2O_7$	100	350	253	[S15]
$Mn_{1.93}P_2O_{7-y}$	**1000**	**600**	**345.6**	**This work**

EIS section

The formula for the lithium ion diffusion coefficient (D_{Li^+}) is as follows:

$$D_{Li^+}=R^2T^2/2S^2n^4F^4C^2\sigma_w^2 \quad (1)$$

$$Z_{re}=R_s+R_{ct}+\sigma_w\omega^{-1/2} \quad (2)$$

Where D and T stand for the Li^+ diffusion coefficient and thermodynamic temperature (298.15 K), respectively, C is the concentration of Li^+, n signals the number of electrons transferred per $Mn_{1.93}P_2O_{7-y}$ molecule at the insertion of Li^+, F denotes the Faraday constant (96485 C mol^{-1}), S mean the surface area of active

electrode, R signifies the gas constant (8.314 J mol^{-1} K^{-1}), ω and σ are the angular frequency and Warburg impedance coefficient, respectively, the latter can be calculated by equation (2) [S16]. Relevant data can be seen in **Table S7**. The calculated lithium-ion diffusion coefficients of $Mn_{2-y}P_2O_{7-y}$ series samples are 3.59×10^{-15}, 8.36×10^{-15}, 8.60×10^{-15}, 1.64×10^{-14}, 5.24×10^{-12} and 8.43×10^{-13} cm^2 s^{-1}, respectively. Amongst them, $Mn_{1.93}P_2O_{7-y}$ possesses higher Li^+ diffusion coefficient and faster charge-discharge process, both of these contribute to its optimal electrochemical performances.

Table S7 Fitting data for $Mn_{2-x}P_2O_{7-y}$.

Samples	$R_s(\Omega)$	$R_{ct}(\Omega)$	W_o-$R(\Omega)$	σ_w (Ω cm^2 $s^{-0.5}$)	D_{Li}^+(cm^2 s^{-1})
$Mn_2P_2O_{7-y}$	4.69	399.40	3.80	390.95	3.59×10^{-15}
$Mn_{1.99}P_2O_{7-y}$	7.38	322.00	3.64	256.18	8.36×10^{-15}
$Mn_{1.97}P_2O_{7-y}$	2.03	156.50	3.49	252.58	8.60×10^{-15}
$Mn_{1.95}P_2O_{7-y}$	3.42	111.90	2.13	183.23	1.64×10^{-14}
$Mn_{1.93}P_2O_{7-y}$	2.34	19.82	0.37	10.24	5.24×10^{-12}
$Mn_{1.91}P_2O_{7-y}$	6.22	47.00	1.37	25.52	8.43×10^{-13}

R_s: solution impedance, **R_{ct}**: charge transfer impedance, **σ_w**: Warburg impedance, **D_{Li}^+**: lithium-ion diffusion coefficient.

References：

[S1] P. Gao, Z. Chen, Y.X. Gong, R. Zhang, H. Liu, P. Tang, X.H. Chen, S. Passerini, J.L. Liu, The role of cation vacancies in electrode materials for enhanced electrochemical energy storage: synthesis, advanced characterization, and fundamentals, Advanced Energy Materials, 10(14)(2020) 1903780-1903804.

[S2] N. Zhang, F.Y. Cheng, Y.C. Liu, Q. Zhao, K.X. Lei, C.C. Chen, X.S. Liu, J. Chen, Cation-deficient spinel $ZnMn_2O_4$ cathode in $Zn(CF_3SO_3)_2$ electrolyte for rechargeable aqueous Zn-ion battery, Journal of the American Chemical Society, 138(39)(2016) 12894-12901.

[S3] B. Koo, S. Chattopadhyay, T. Shibata, V.B. Prakapenka, C.S. Johnson, T. Rajh, E.V. Shevchenko, Intercalation of sodium ions into hollow iron oxide nanoparticles, Chemistry of Materials, 25(2)(2013): 245-252.

[S4] B. Koo, H. Xiong, M.D. Slater, V.B. Prakapenka, M. Balasubramanian, P. Podsiadlo, C.S. Johnson, T. Rajh, E. V. Shevchenko, Hollow iron oxide nanoparticles for application in lithium ion batteries, Nano letters, 12(5)(2012), 2429-2435.

[S5] T. Hu, J. Yang, X. Wang, Carbon vacancies in Ti_2CT_2 MXenes: defects or a new opportunity? Physical Chemistry Chemical Physics, 19(47)(2017):31773-31780.

[S6] H. Wang, J.J. Zhang, X.D. Hang, X.D. Zhang, J.F. Xie, B.C. Pan, Y. Xie,

Half-metallicity in single-layered manganese dioxide nanosheets by defect engineering, Angewandte Chemie, 127(4)(2015), 1211-1215.

[S7] F.Y. Li, Y. Anjarsari, J.M. Wang, R. Azzahiidah, J.Z. Jiang, J. Zou, K. Xiang, H.J. Ma, Arramel, Modulation of the lattice structure of 2D carbon-based materials for improving photo/electric properties, Carbon Letters, 33(5)(2023), 1321-1331.

[S8] W. Zhang, W.C. Lu, H.X. Zhang, K.M. Ho, C.Z. Wang, Lattice distortion and electron charge redistribution induced by defects in graphene, Carbon, 110(2016) 330-335.

[S9] T.F. Wu, G.L. Dai, C.C. Qin, J.L. Cao, Y.F. Tang, Y.F. Chen, A novel method to synthesize SnP_2O_7 spherical particles for lithium-ion battery anode, Ionics, 22 (2016) 2315-2319.

[S10] J.Y. Zhang, J.F. Zhang, J. Liu, Y. Cao, C.C. Huang, G.J. Ji, Z.W. Zhao, X. Ou, B. Zhang, Environmentally phase-control stratagem for open framework pyrophosphate anode material in battery energy storage, Journal of Materials Chemistry C, 9(29)(2021) 9147-9157.

[S11] M.Y. Pan, S.T. Lu, Y.Y. Li, C. Li, K.Z. Cao, Y. Fan, Copper hydroxyphosphate $Cu_{2(}OH)PO_4$ as conversion-type anode material for lithium-ion batteries, Ionics, 29(6)(2023) 2209-2215.

[S12] R. Essehli, B. El Bali, A. Faik, M. Naji, S. Benmokhtar, Y.R. Zhong, L.W. Su, Z. Zhou, J. Kim, K. Kang, M. Dusek, Iron titanium phosphates as high-specific-capacity electrode materials for lithium ion batteries, Journal of

Alloys and Compounds, 585(2014) 434-441.

[S13] V. Mani, N. Kalaiselvi, $LiVP_2O_7$/C: a new insertion anode material for high-rate lithium-ion battery applications, Inorganic Chemistry, 55(8)(2016) 3807-3814.

[S14] S.Q. Wang, X.Y. Jiang, G.D. Du, Z.P. Guo, J.Y. Jang, S-J. Kim, Solvothermal synthesis of $Mn_2P_2O_7$ and its application in lithium-ion battery, Materials Letters, 65(21-22)(2011) 3265-3268.

[S15] F.F. Li, Z.H. He, J.F. Gao, L.B. Kong, The investigations of pyrophosphate $CoNiP_2O_7$ produced by hydrothermal process: a high-performance anode electrode material for Li-ion hybrid capacitor, Ionics, 26(2020) 2989-3001.

[S16] C. Li, J. Mao, Ex-situ study on the structure changes of $Li_4Ti_5O_{12}$-based anode materials under different lithium insertion amounts, Journal of Solid State Chemistry, 296(2021) 121974-121981.